BNL 28195

CONF-800684--7

OG 544

MASTER

Optical Fibers and Avalanche Photodiodes for Scintillator Counters

S.R. Borenstein[1], R.B. Palmer and R.C. Strand
Physics Department, Brookhaven National Laboratory,
Upton, New York 11973

Invited talk

at the International Conference on

Experimentation at LEP

University of Uppsala, Sweden
16-20 June, 1980

[1]University Affiliation: York College, CUNY, New York, N.Y.

DISCLAIMER

Optical Fibers and Avalanche Photodiodes for Scintillator Counters

Invited talk at the International Conference on

Experimentation at LEP

University of Uppsala, Sweden
16-20 June, 1980

S.R. Borenstein[1], R.B. Palmer and R.C. Strand
Physics Department, Brookhaven National Laboratory,
Upton, New York 11973

Abstract

Optical Fibers and Avalanche Photodiodes for Scintillator Counters. S.R. Borenstein, R.B. Palmer and R.C. Strand (Physics Department, Brookhaven National Laboratory, Upton, New York) Physica Scripta (Sweden).

Fine hodoscopes can be made of new scintillating optical fibers and one half inch end-on PMT's. An avalanche photodiode with small size and immunity to magnetic fields remains as a tempting new device to be proven as a photodetector for the fibers.

[1]University Affiliation: York College, CUNY, New York, N.Y.

INTRODUCTION

I. Fine Scintillation Detectors for Hadron Storage Accelerators

When the luminosity of the ISABELLE (400 x 400 GeV) storage accelerator reaches 2 x 10^{32} $cm^{-2}sec^{-1}$, there will be 10^7 pp interactions per second expected with an average of 20 charged secondaries going mostly forward where up to 2 x 10^{12} particles $sec^{-1}sr^{-1}$ are expected. At most of the production angles secondary intensities are more tolerable. Between 5.7° (100 mrad) and 45° 80 Mhz sr^{-1} is expected and between 45° and 135° 2 Mhz sr^{-1} is expected [1].

Count rate capability and space resolution of particle detectors determine the gross size of a magnetic spectrometer. Fine resolution allows short magnetic orbits and high rate capability permits tracking to start close to the origin. The volume and the total cost of a spectrometer scale up rapidly as the cube of the linear dimensions required. Track chambers and segmented calorimeters for use in magnetic fields should facilitate efficient use of these more costly volumes.

High rate particle detectors can be made from scintillating optical fibers and silicon photodiodes. They would be compact and undisturbed by magnetic fields. A fiber hodoscope near the origin could initiate particle tracking. Cooled avalanche photodiodes (APD's) are promising photon-counters for the scintillating optical fibers that have been developed.

II. Scintillating Optical Fibers: Excitation with 3.5 MeV/c Electrons

The core of a round scintillating fiber is drawn from a heated preform that is a polished, circular cylinder of PVT scintillator. An outer cladding is applied to the optically smooth surface of the core as it emerges from the oven. The cladding has a lower index of refraction than the core,

so forward and backward cones of photons are captured by "total" internal reflection. The loss of a small fraction of the photons from the light guide is characterized by an attenuation length. A sketch of a scintillating optical fiber appears in Figure 1.

Bare scintillating fibers capture more light but they acquire attenuating surface defects through handling and exposure. Clad fibers fit into small spaces without extra material for their protection.

BNL entered into a contract with Calileo Electro-Optical Corporation [2] to produce optical fibers using NE102 and NE110 scintillator cores and a proprietary ultra-violet curing polymer as the cladding. The NE102 and NE110 are scintillators provided by Nuclear Enterprises, Inc. Since March 1979 we have been testing the performance of these fibers at BNL.

The tests include attaching the fiber to a PMT, irradiating the fiber (at some distance away from the PMT) with minimum ionizing electrons from Ruthenium 106 and analyzing the resultant pulse spectrum. We refer to the pulse to be analyzed as S. The analyzer is gated by a coincidence pulse from two small scintillator chips which sandwich the fiber. Thus, the two chip counters which we refer to as T_1 and T_2 serve to define an electron trajectory which had a high probability of intersecting the fiber. The efficiency is defined as the coincidence ratio $S \cdot T_1 \cdot T_2 / T_1 \cdot T_2$. The discriminator for S is set below the threshold for single photoelectrons. The experimental setup is shown schematically in Figure 2(a). Figure 2(b) shows some plausible electron trajectories. Due to coulomb scattering as well as misalignment of the elements, it is possible for the electron to go through T_1 and T_2 and nevertheless miss the fiber. Thus we expect that the efficiency will have some upper limit.

The performance of the fiber is given by the light yield and the efficiency as a function of distance from ionizing electron to PMT. The charge spectrum is characterized by a very sharp initial peak, the pedestal, followed by a broad peak at the mean number of photoelectrons times the gain of the PMT. The position of the peak relative to the pedestal is a measure of the total charge delivered by the anode of the PMT, which is in turn a measure of the number of photoelectrons produced at the cathode. As the light intensity increases, the mean increases.

The next step is to calibrate the analyzer in terms of channels per photoelectron. An accurate determination is obtained by using a phototube with a high gain first dynode which resolves the first, second, etc. photoelectron peaks. Our tests were performed with an EMI type 9843 or a RCA type 8850 photomultiplier tube. In Figure 4(a) we see a clear separation between 1 and 2 photoelectrons obtained from a low level scintillation signal. As expected, the position of the peaks is linear in channels. This method allows us to calibrate our spectra in photoelectrons, independently of the operating voltage of the PMT or the gain of all associated electronics. The most accurate determination is obtained from the mean of the distribution. However, ratios of the heights of the peaks are a useful measure of the average number of photoelectrons.

We analyzed several lengths of 1 mm diameter NE110 fiber, and the results are shown in Fig. 3(a). To expedite the data taking we glued most fibers to the PMT with quick drying epoxy cement. However, for one sample, data was taken using optical cement. The extra data point at 40 cm shows that we may expect about a 40% increase in photoelectron yield by properly matching the fiber to the PMT.

The attenuation curve consists of two regions. The first region out to about 20 or 30 cm is characterized by rapid attenuation due to rapid absorption of ultra-violet photons and due to a large acceptance by the cladding - air surface. Beyond about 30 cm, where the very short wave photons and the extra acceptance are no longer contributing, the attenuation is well described by a single attenuation length of about 130 cm for NE110.

The vertical scale of Figure 3(a) is photoelectrons. A quantum efficiency of about 20% is estimated by convoluting the emission spectrum of NE110 with the spectral efficiency of the photocathode. Thus the scale of Figure 3(a) should be multiplied by 5 to estimate the number of photons surviving a given length of fiber. As an example, a 50 cm length of fiber produces at least 23 photons, and perhaps as many as 30 if an optical cement is used. This implies a detection efficiency of at least 99%. At one meter these figures are 15 and 21 photons, respectively, implying an efficiency between 95 and 98.5%

As a further indication that we have correctly estimated the number of photoelectrons, we can calculate the probability that a signal whose average value is $\langle n \rangle$ photoelectrons, will actually be detected by the PMT. This ability is just $1 - e^{-\langle n \rangle}$. The efficiency described earlier as the coincidence ratio $S \cdot T_1 \cdot T_2 / T_1 \cdot T_2$ has a maximum value which we may call the geometric limit. This maximum value, about 85%, is the value obtained when the fiber is so short that there is virtually no chance that the beta particle could go through the fiber without giving a large signal. The true efficiency is obtained from the ratio of the measured efficiency to the geometric limit.

Figure 3(b) is a plot of the true efficiency vs. fiber length. The curve is the theoretical value $1 - e^{-\langle n \rangle}$, where $\langle n \rangle$ has been obtained from Figure 3(a). The agreement between the curve and the experimental points corresponds to an uncertainty of about ±12% in the photoelectron scale.

Figure 4 shows a series of spectra taken with two fibers, one NE102 and the other NE110, glued to the same RCA type 8850 PMT. The NE102 gave more light at less than 40 cm and the NE110 gave more light at greater than 40 cm.

Several samples of NE110 fiber were tested. The diameter is 1.2 ± .1 mm. The attenuation length is 1.3 ± .2 m and the associated effective yield at the origin is 8 ± 2 photoelectrons.

III. Scintillating Optical Fibers: Excitation with 3.0 GeV/c Negative Pions

To compare the response of a fiber to pions with the response to electrons, negative pions from the Brookhaven AGS and negative electrons from ^{106}Ru were used to excite the same fiber in the same geometry with the same trigger. The respective whole fiber spectra in Figure 5 both correspond to an average number of 3.7 photoelectrons at 30 cm from the beam. The optical greased coupling is less efficient than a glued coupling that collects an average of 7.0 p.e.-to-electrons at 30 cm as shown in Figure 5. The equivalence of electron and pion excitation enables us to continue many studies when accelerator time is not available, and to use with more confidence the yields and attenuation lengths from electrons in the study of pion excitations.

A pion is a much finer probe than a coulomb scattered electron to measure the photon yield as a function of distance from the edge of the fiber. A small

beam of pions was triggered by the horizontal overlap of two small scintillation counters. One of them was moved with a micrometer screw so the amount of overlap could be selected. The single fiber was mounted vertically in a light tight compartment, which we call the tower, that was carried on a moving stage as shown in Figure 6. Stage coordinates were obtained from a precise lead screw with a pitch of one mm. Readout was from a handwheel that had 500 divisions. Backlash in the stage coordinate was eliminated with a return spring.

Each end of the fiber was coupled to a PMT with optical grease. Two and one half cm below the fine beam a one-half inch Hamamatsu type R647-4PMT was coupled. Thirty cm above a RCA type 8850 PMT was used. Photoelectron yields and efficiencies were measured with the upper PMT.

The trigger counters were overlapped by 0.3 mm. They were gated by upstream counters in the beam transport and by a one mm wide downstream counter just after the tower. This last counter eliminated most of the two-particle triggers that missed the fiber. Upstream knock-on electrons were suspected as a major cause of these doublets. The efficiency of the fiber at the upper PMT for this trigger was measured. In Figure 7 the profile in stage coordinates shows a peak efficiency of 70 percent. This profile implies that the active fiber is 1.18 ± .04 mm wide and that the probe is 0.29 ± .04 mm wide. Direct micrometer measurements of these widths are 1.25 and 0.3 mm.

Next, the two trigger counters were separated by .3 mm and the profile for this accidental trigger was obtained as shown in Figure 7. Since the same types of accidental events are present in the real triggers, the qualitative character of the real profile is confirmed. A detailed unfolding of the accidental profile from the observed profile is compatible with 100% efficiency at the top of the corrected profile.

In order to probe selected horizontal apertures within the fiber, the lower PMT was included in the trigger. The enhanced yield near the origin in Figure 3 allowed the lower PMT to be an unbiased trigger for photons in the fiber. When the fiber was centered on the probe, the efficiency was 98 percent. This corresponds to average pulses of 3.9 photoelectrons at the upper PMT. This yield is confirmed by the corresponding pulse height spectrum shown in Figure 8 that indicates an average pulse of 3.7 photoelectrons. As the fiber is moved away from the center of the probe, the efficiency falls as fewer photoelectrons per trigger are realized. This reduced yield is confirmed by the pulse height spectrum shown in Figure 8 where an average of 3.0 photoelectrons are observed. The central 0.6 mm of horizontal aperture is studied this way. The observed efficiency profile is compatible with light yields that are proportional to the length of the pion trajectory within the fiber. Hence we can calculate the amount of overlap required for a given detection efficiency in a two layer hodoscope that is constructed from these round fibers.

IV. Counting Bursts of Photons: Photomultiplier Tubes or Photodiodes

The photon counter converts single photons into single electrons with its characteristic quantum efficiency and detects bursts of photoelectrons with the Poisson efficiency. Since we have measured the yield and attenuation character of scintillating fibers, we can calculate the particle detection efficiency of a given photon counter with a given length and fractional width of the fiber.

Arrays of half inch end-on PMT's such as the Hamamatsu R647-04 with the half inch bias circuit can service fiber light guides if adequately shielded from magnetic fields. Gordon [3] has shown that this PMT is suitable for a segmented calorimeter. A low-loss fiber light guide, that is as tolerant of radiation

as scintillators, needs to be realized.

High quantum efficiency, small size, and immunity to magnetic fields have kept avalanche photodiodes (APD's) [4] in the competition for photodetectors. Although they have higher quantum efficiencies than PMT's, they cannot count single photons because of the spread in their gain distribution. With the somewhat more generous photon yields, calorimeters have remained an attractive source for APD's, cooled APD's, or cooled PIN's (unity gain photodiodes), with ultra quiet - fast preamplifiers.

Photodiode packages are small enough to be attached to the ends of scintillating fibers via their entrance windows. On the inside of the package the photodiode is attached to the entrance window for maximum efficiency.

The entrance window could be a Winston [5] cone in order to reduce the diameter of the APD. A smaller APD is less expensive, quieter, and faster. It has a higher manufacturing yield, a lower dark current, and a lower capacitance.

V. The Silicon Reach-Through APD

The quantum efficiency [6] of silicon diodes is eighty percent for the emission spectrum of NE102 as shown in Figure 9. This is about four times better than the quantum efficiency of our PMT's.

The internal electric field of a silicon reach-through APD (RAPD) has a sharp spike at one side of the chip and a long plateau that reaches through to the other side. In the RCA architecture [7] of the RAPD, photons are absorbed in the intrinsic substrate where the field of the reach-through plateau

sweeps the photoelectrons through to the narrow avalanche gain region of the electric field spike.

These devices are made by diffusing a thin p-layer on the entrance side and a deep p-layer followed by a shallow n-layer on the high field side of a thin wafer of intrinsic silicon. Photons enter through the thin p-layer and photoelectrons arrising in the intrinsic region initiate avalanche gain at the field spike of the n-p junction. RAPD's up to 5 mm in diameter have been made by RCA. The dimensions of the RAPD package can be as small as $(5\ \text{mm})^3$.

The best sensitivity is obtained when a charge sensitive preamplifier is placed close to the RAPD to minimize stray capacitance at the input. Signals from a low noise preamplifier were sent to a gaussian shaping amplifier that completed the charge measurement. The optimal shaping time was 0.5 nsec. Noise in the gain of the RAPD increases with gain so there's an optimal gain for each input signal level that gives the best signal to noise ratio. Fortunately, the dark noise has a broad minimum as a function of gain and the optimal shaping time changes slowly with gain.

We have tested one mm and three mm RCA diodes in the linear mode at temperatures between 77 and 300°K. A reverse bias of a few hundred volts controls gains between 10 and 100 at room temperatures. A modest amount of cooling to zero degrees centigrade reduces the dark noise to eight photoelectron rms for a one mm RAPD as shown in Figure 10.

At BNL a quieter and faster preamplifier is being developed [8] with a low noise gallium arsenide field effect transistor. The APD's capacitance must be comparable to the GaAs FET's capacitance to achieve the most improvement.

A Winston [5] cone to couple the scintillating fiber to the APD could reduce the size and capacitance of the APD. The APD would be glued to the exit of the Winston cone. The diameter of the exit could be three times smaller than the diameter of the entrance without loss of photons because our scintillating fibers have a low numerical aperture.

VI. Counting Photons with the RCA Avalanche Photodiode in the Breakdown Mode

This year RCA realized [9] a photon counting mode with their standard RAPD. It is cooled to reduce the dark current and biased beyond the breakdown voltage. The gain of an APD diverges as its breakdown voltage is approached from below. The difference between the operating voltage and the breakdown voltage is called the overvoltage. Upon entering the electric field spike at the np-junction, a single photoelectron or thermal electron triggers a fast discharge if the overvoltage is high enough. The size of the discharge is proportional to the overvoltage. The dark count rate depends on the true counting rate and the overvoltage. The discharge seems to excite some metastable states that decay some random time later and retrigger the discharge. Low overvoltages which might fill fewer of these electron traps also might permit some single photoelectrons to pass the np-junction without initiating a discharge.

We have just begun to operate one of our RAPD's in the breakdown mode at temperatures between $-80^{\circ}C$ and $-130^{\circ}C$. Scintillation pulses and LED pulses have been observed. We will seek a combination of temperature and overvoltage that gets a dark rate which is useful for a real hodoscope.

ACKNOWLEDGEMENTS

The detectors for this work were constructed by E. Frantz, G. Mayman and J. Scheliga. The cryostat for cooling the APD's was borrowed from H. Kraner of the BNL Instrumentation Division. The test beam at the AGS was provided by T. Ludlam, D. Krause and J. Renardi. Helpful discussions with R. Boie, R. DiNardo, H. Gordon, V. Radeka, P. Rehak and J. Sondericker contributed ideas and encouragement for this research.

This research was supported by the U.S. Department of Energy under Contract No. DE-AC02-76CH00016.

REFERENCES

[1] Marx, J. and Ozaki, S., Topic I: Detectors and Experiments, Summary of Activity, Proc. 1977 ISABELLE Summer Workshop, BNL 50721, p. 4.

[2] BNL Contract #463787-S with Galileo Electro-Optical Company.

[3] Cordon, H.A., New Ideas on Calorimeters, submitted to these Conference Proceedings.

[4] Strand, R., Avalanche Photodiodes for ISABELLE Detectors, Proc. 1978 ISABELLE Summer Workshop, BNL 50885, p. 33.

[5] Hinterberger, H. and Winston, R., Rev. Sci. Instr. 39, 419 (1968).

[6] McIntyre, R.J., Final Report to BNL: Feasability Study on the use of APD's with Scintillators, Sept. 1978.

[7] Webb, P.P., McIntyre, R.J., Conradi, J., RCA Review, 35 (1974).

[8] Boie, R., BNL Instrumentation Division, private communication.

[9] McIntyre, R.J., private communication.

FIGURE CAPTIONS

Fig. 1 Schematic diagram for a scintillating optical fiber.

Fig. 2 (a) Apparatus for analyzing charge spectrum of scintillating fibers (b) Detail of apparatus showing electron trajectories. Both scattering and counter misalignment have been exaggerated for purpose of illustration.

Fig. 3 Attenuation curves for 1 mm diameter NE110 fiber.

Fig. 4 Direct comparison of spectra of NE102 and NE110 fibers using RCA8850 PMT.

Fig. 5 Comparative charge spectra for 30 cm of a 1 mm NE110 fiber that was coupled to a PMT with optical grease and exposed to

(a) 3 GeV/c negative pions

(b) 3.5 MeV/c betas from ^{106}Ru

Charge spectrum for 30 cm of another 1 mm NE110 fiber that was coupled to a PMT with glue and exposed to

(c) 3.5 MeV/c betas from ^{106}Ru.

Fig. 6 Photograph of a device for testing scintillating fibers in a pion beam.

Fig. 7 Efficiency profile of a 1 mm NE110 fiber at 30 cm for 3 GeV/c pions and a 0.3 mm probe:

(a) Real triggers

(b) Accidental triggers

Fig. 8 Charge spectra for a 1 mm NE110 fiber at 30 cm for 3 GeV/c pions and a 0.3 mm probe:

(a) Fiber centered on the probe

(b) Fiber edge centered on the probe

Fig. 9 (a) Quantum efficiency of a RCA reach through APD that is optimized for scintillator light (b) Emission spectrum of NE102 scintillator.

Fig. 10 Behavior of a 1 mm RCA reach through APD at a gain of 25 as a function of temperature:

(a) Rms signal resolution for 70 photoelectrons and 0.5 nsec gaussian shaping

(b) Rms dark noise for 0.5 nsec gaussian shaping

(c) Dark current.

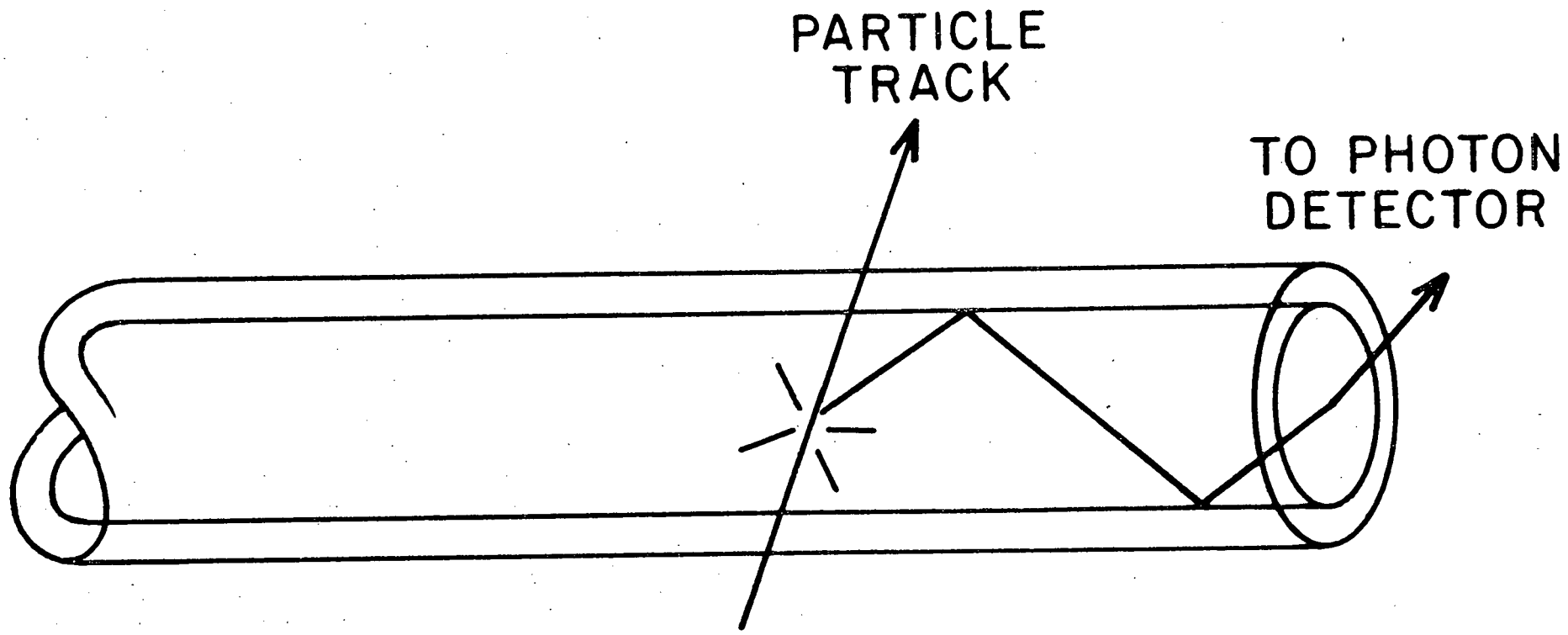

Figure 1

APPARATUS FOR ANALYZING PULSE HEIGHT SPECTRUM
OF SCINTILLATING FIBER

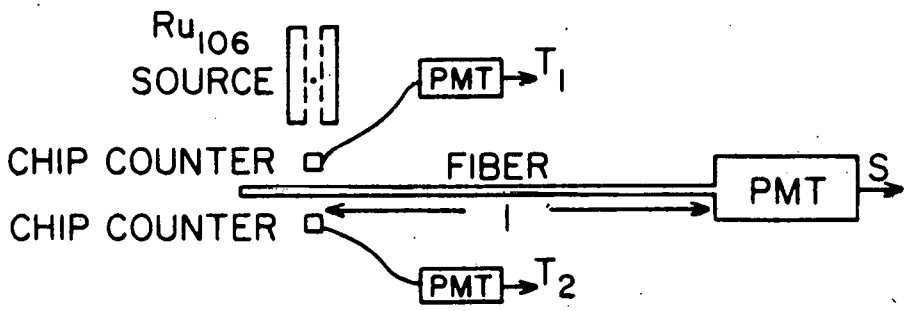

(a) SCHEMATIC

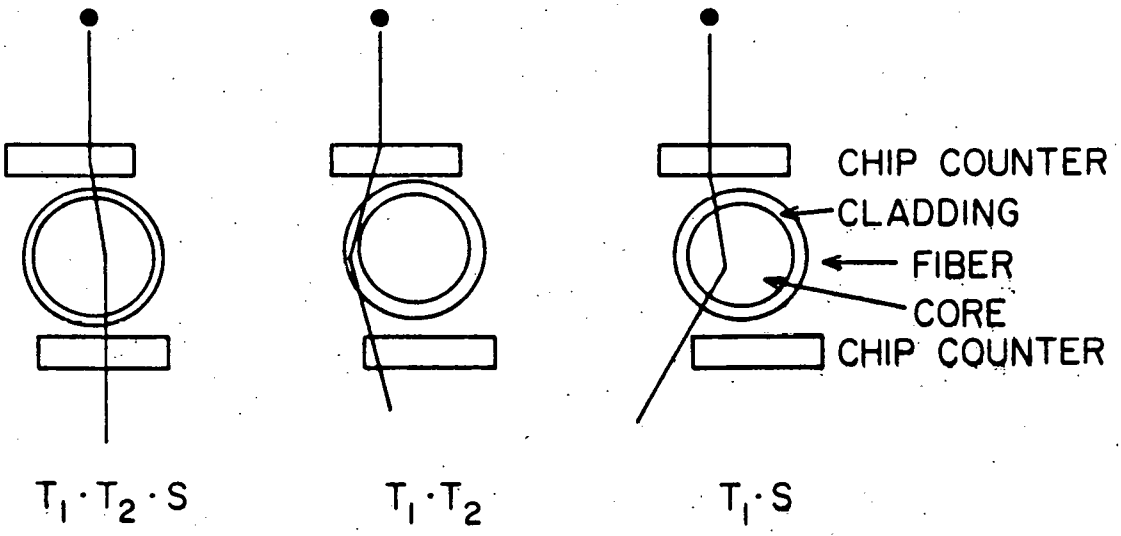

(b) CLOSE UP VIEW OF ELECTRON TRAJECTORY

Figure 2

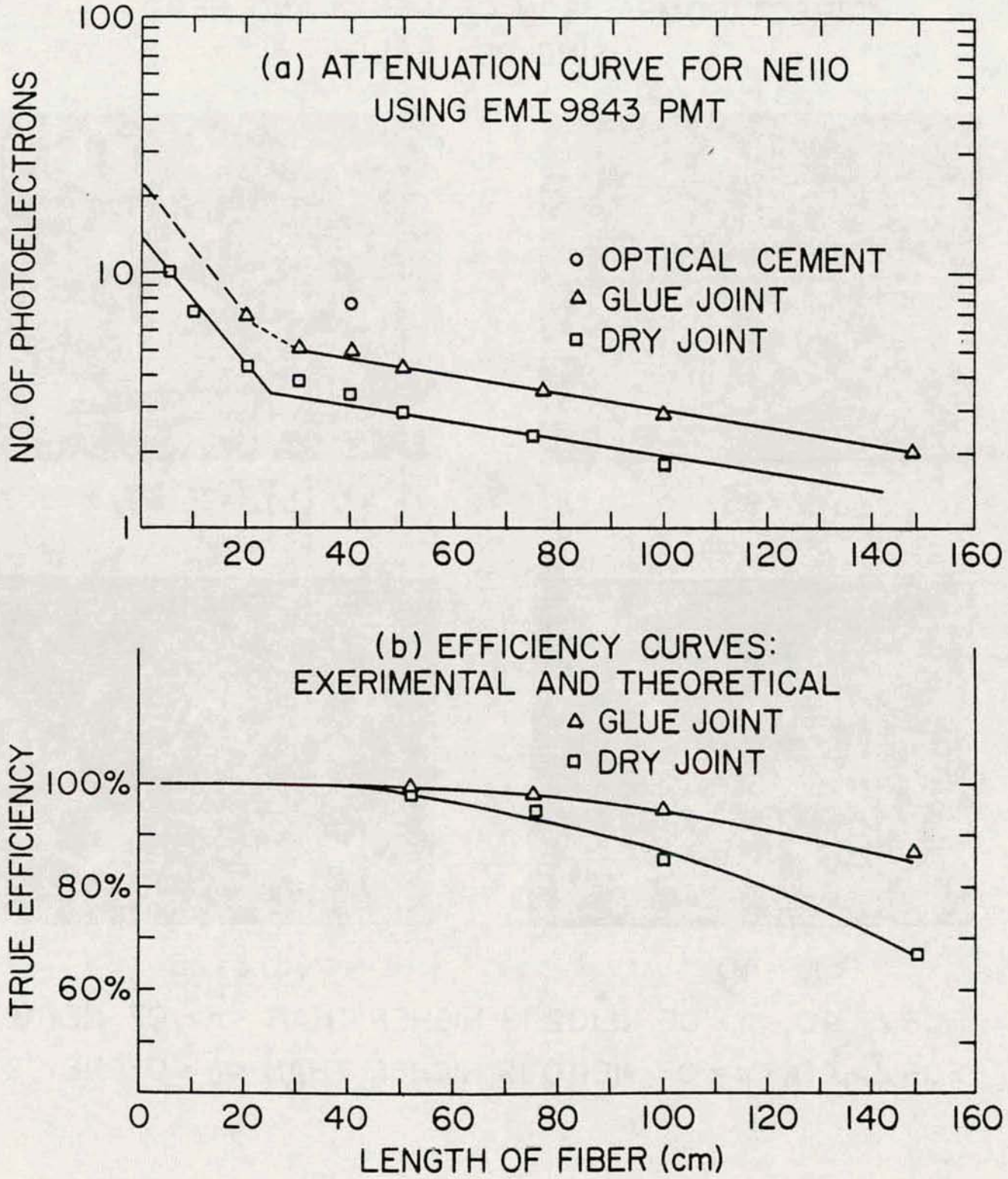
(a) ATTENUATION CURVE FOR NE110
USING EMI 9843 PMT
NO. OF PHOTOELECTRONS
100
10
1
OPTICAL CEMENT
GLUE JOINT
DRY JOINT
20
40
60
80
100
120
140
160
(b) EFFICIENCY CURVES:
EXERIMENTAL AND THEORETICAL
GLUE JOINT
DRY JOINT
TRUE EFFICIENCY
100%
80%
60%
0
20
40
60
80
100
120
140
160
LENGTH OF FIBER (cm)

Figure 3

DIRECT COMPARISON OF NE102 AND NE110
USING RCA 8850

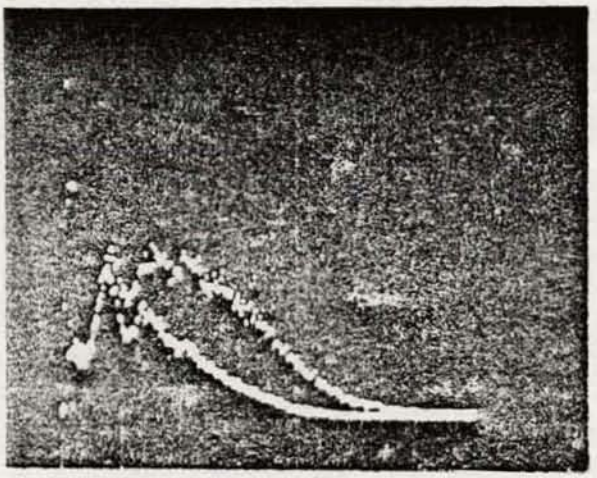

(a) $\ell = 95$

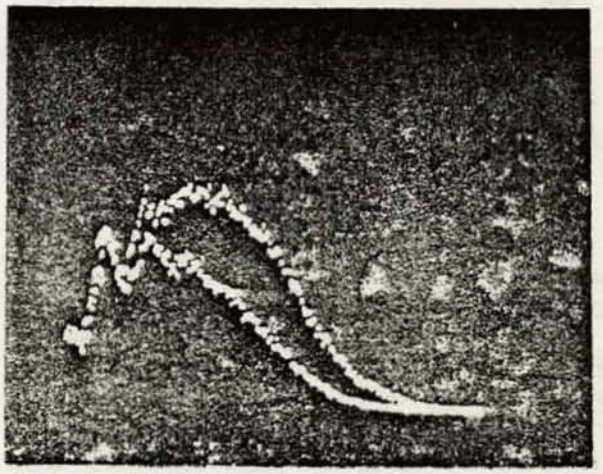

(b) $\ell = 75$

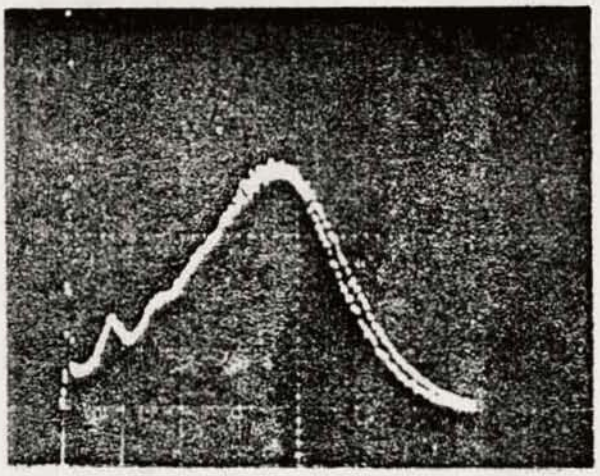

(c) $\ell = 40$

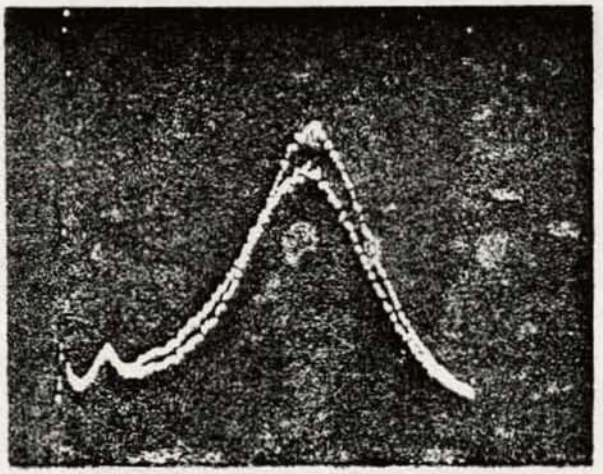

(d) $\ell = 25$

FOR $\ell < 40$, <n> OF NE102 IS HIGHER THAN <n> OF NE110

FOR $\ell > 40$, <n> OF NE110 IS HIGHER THAN <n> OF NE102

Figure 4

FIBER AND BEAM COMPARISONS FOR 30cm LENGTH

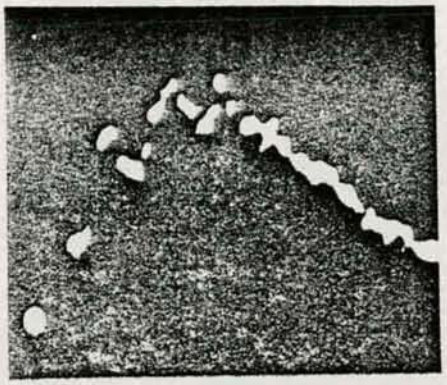

FIBER EXPOSED TO π BEAM
GREASE JOINT TO PMT

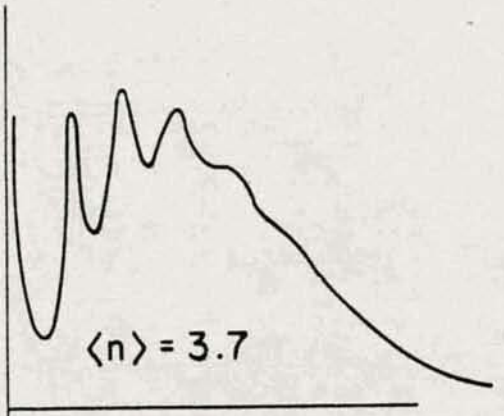

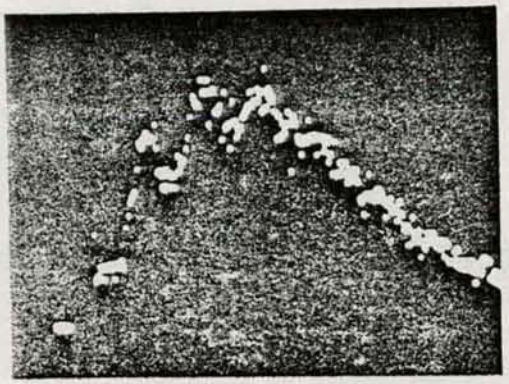

SAME FIBER EXPOSED TO ELECTRONS
UNDER IDENTICAL CONDITIONS

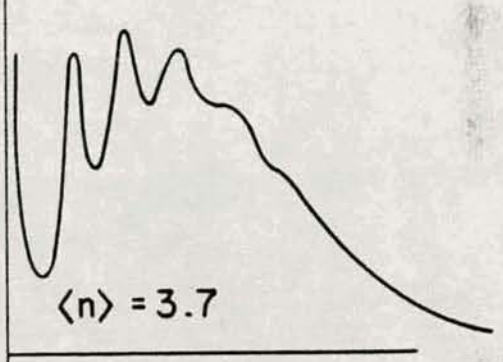

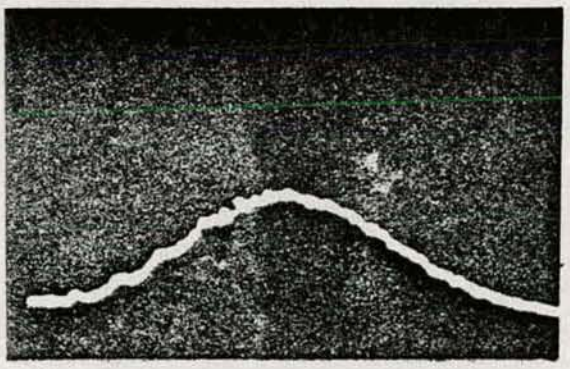

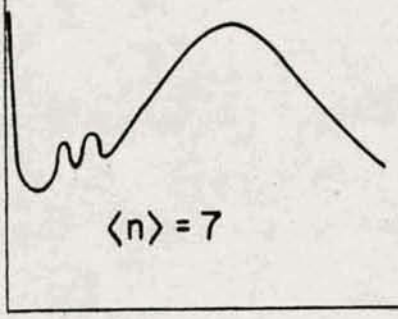

DIFFERENT FIBER EXPOSED TO ELECTRONS
GLUED TO PMT

Figure 5

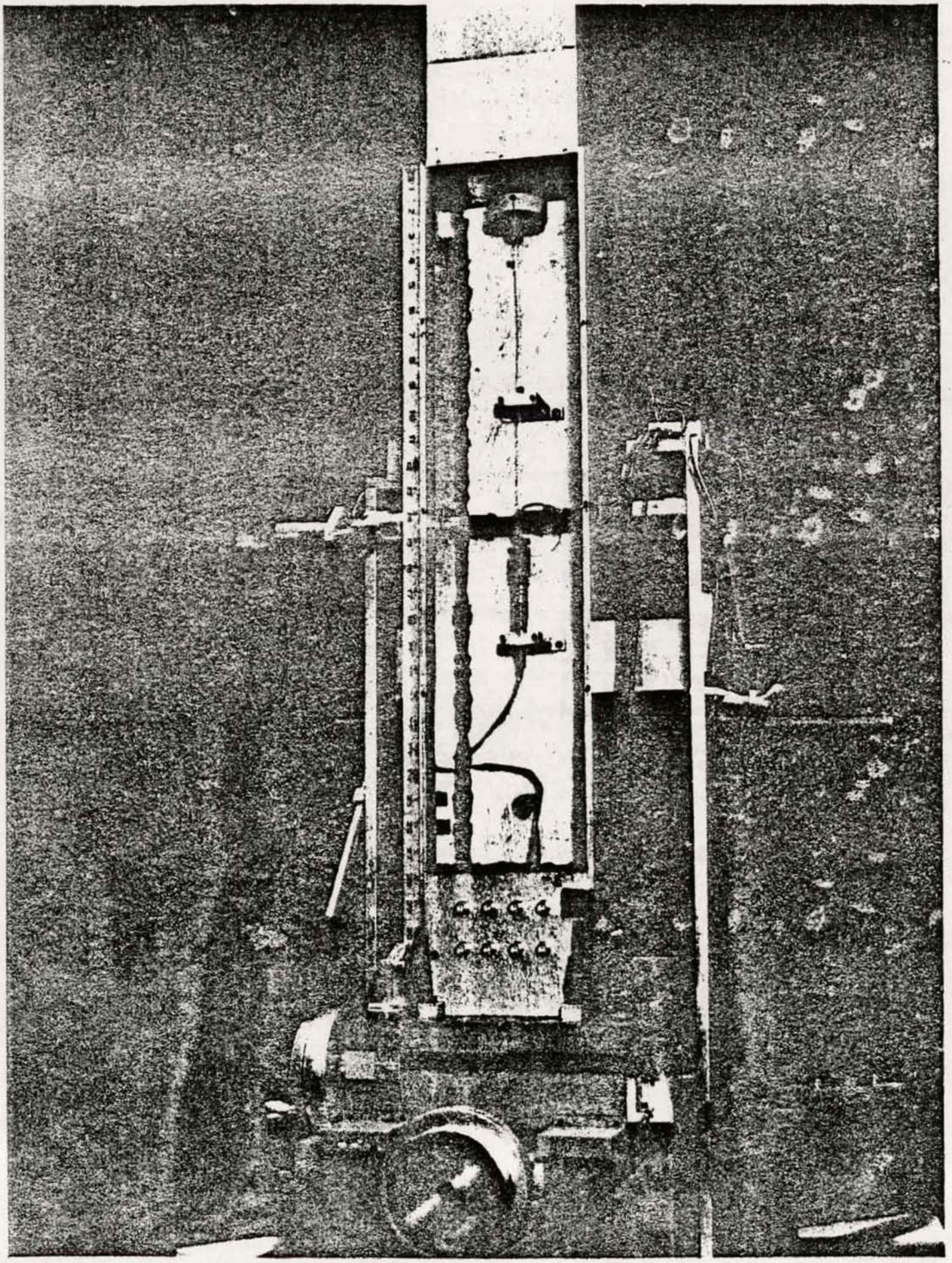

Figure 6

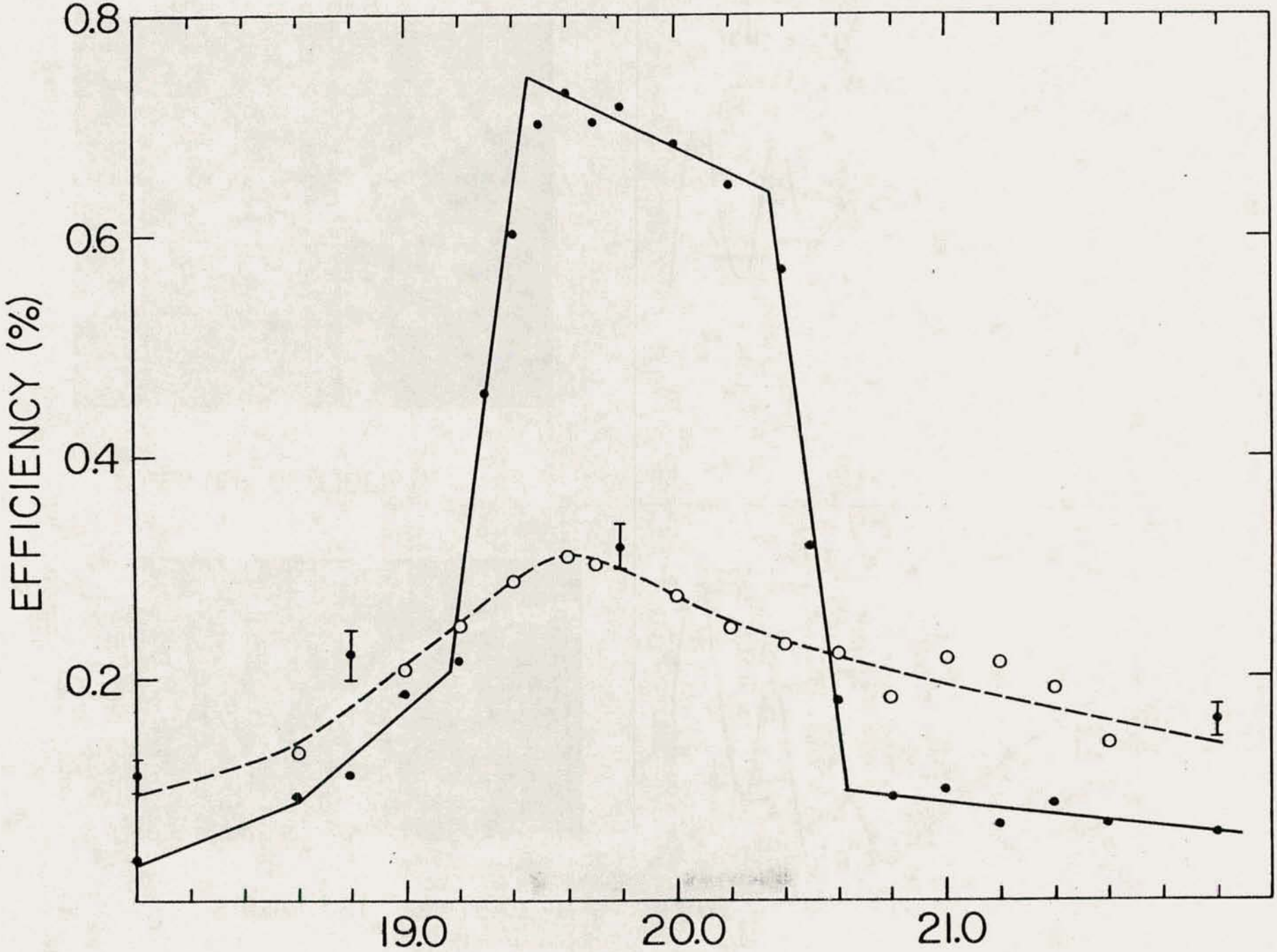

Figure 7

SIGNAL = SI GATE = $T_1 \cdot T_2 \cdot S_2 \cdot$ BEAM

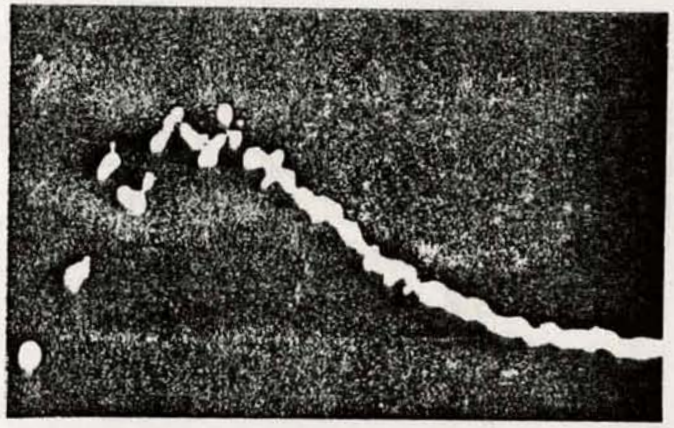

CENTER OF FIBER

EDGE OF FIBER

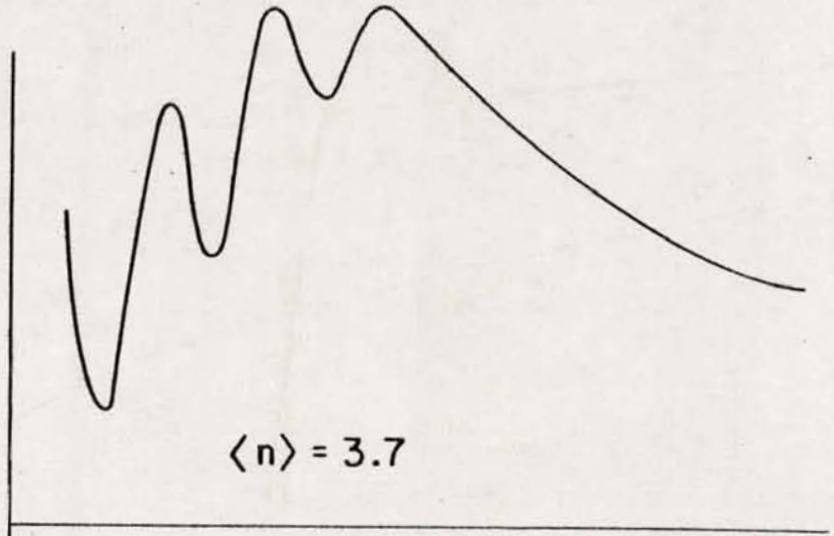

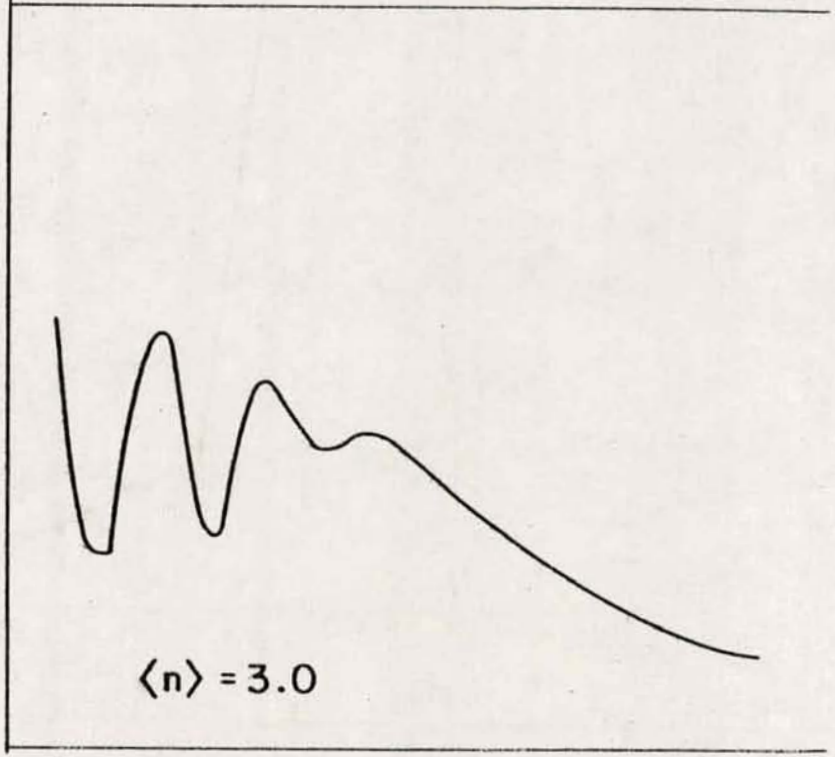

Figure 8